Paraxial ray tracing for atmospheric wave propagation

J. Virieux, Nicolas B. Garnier, E. Blanc, J.-X. Dessa

Paraxial ray tracing for atmospheric wave propagation

J. Virieux,[1] N. Garnier,[2,3] E. Blanc,[3] and J.-X. Dessa[4]

Received 13 May 2004; revised 18 August 2004; accepted 27 September 2004; published 21 October 2004.

[1] Ray tracing for sonic wave propagation in a two-dimensional atmosphere structure is performed in the presence of spatially variable wind by using an Hamiltonian approach. Paraxial ray tracing is deduced by first-order perturbations. Using standard atmospheric data or illustrative models, we test numerically the Hamiltonian approach. The ray tracing allows accurate estimation of trajectories and associated travel-times as well as stable and accurate amplitude variations along a ray. Lateral variations of both sonic and wind velocity are important for quantitative evaluation of acoustic waves. Gradients of the wind field must be taken into account for precise quantification of ray trajectories and, consequently, for the localization of ground impacts, a key element for any micro-barometric recording station. *INDEX TERMS:* 0689 Electromagnetics: Wave propagation (4275); 3367 Meteorology and Atmospheric Dynamics: Theoretical modeling; 3384 Meteorology and Atmospheric Dynamics: Waves and tides; 0350 Atmospheric Composition and Structure: Pressure, density, and temperature; 0399 Atmospheric Composition and Structure: General or miscellaneous. **Citation:** Virieux, J., N. Garnier, E. Blanc, and J.-X. Dessa (2004), Paraxial ray tracing for atmospheric wave propagation, *Geophys. Res. Lett.*, *31*, L20106, doi:10.1029/2004GL020514.

1. Introduction

[2] The international infrasound detection network dedicated to the control of the Comprehensive Test Ban Treaty (CTBT) has increased substantially the amount of data collected by micro-barometric stations or infrasonic arrays for the detection of eventual atmospheric explosions [*Christie*, 1999]. Different known sources of acoustic waves in the atmosphere exist as rockets or supersonic planes [*Calais and Minster*, 1996; *Le Pichon et al.*, 2002a] meteorites [*Le Pichon et al.*, 2002b] and solar eclipses [*Farges et al.*, 2003]. Earthquakes may also excite acoustic waves in the atmosphere [*Artru et al.*, 2001]. Consequently, we must improve our understanding of the acoustic wave propagation to interpret what we observe with different recording systems on the ground.

[3] The computation of sound wave travel-time and pressure amplitudes in the atmosphere differs significantly from computation in media (as the solid Earth or as different oceanic media) because the time-varying atmosphere properties have wide range of variation within the 200 km depth layer where acoustic waves propagate. It has been shown that the atmospheric wind, which is very strong in the stratosphere, may modify the wave propagation and change significantly the propagation azimuth [*Le Pichon et al.*, 2002a]. Daily as well as seasonal variations are observed. Empirical atmospheric models using global databases obtained from radars, balloons, rockets and satellites provide temperature and wind profiles and their variations [*Hedin et al.*, 1996]. This velocity description allows potentially accurate propagation modeling.

[4] Instead of solving complex fluid mechanics using numerical techniques as finite element/volume approaches which will be of little use for fast warning of possible dangerous sources, we shall consider asymptotic wave propagation. By doing so, we limit our simulation to relatively high frequency waves around few hertz (typically 5 Hz) where gravity influence could be neglected. Attenuation is not considered as well although it should be included in the future.

[5] Following a ray approach as already done for 1D layered structures [*Garcès et al.*, 1998], we investigate the influence of varying sound and wind fields on both ray trajectories (and, consequently, on travel times) as well as on the amplitude of the pressure wave (and, consequently, on neighboring rays). Both geometrical and paraxial ray tracing will be considered for time and amplitude variations [*Abdullaev*, 1993].

2. Ray Tracing Equations in a Moving Medium

[6] We neglect gravitational effects in our high frequency approximation. A sound speed structure $c(x_i, x_j)$ is defined in a 2D Galilean Cartesian system (spherical effects are negligible for distances less than 500 km) where indexes i and j are for each coordinate we consider. The wind velocity $\vec{v}(x_i, x_j)$ varies only in space although time variation may be included if needed. Along rays, travel time $T(x_i, x_j, t)$ is defined by the Eikonal equation

$$\left(\vec{\nabla}T\right)^2 = \frac{1}{c^2\left(x_i, x_j\right)}\left(1 - \vec{v}\left(x_i, x_j\right)\cdot\vec{\nabla}T\right)^2. \qquad (1)$$

[7] The differential equations for the position $\vec{q}$, the slowness vector $\vec{p} = \vec{\nabla}T$ as well as the propagation time T may be expressed in a canonical form [*Courant and John*, 1966]:

$$\frac{dq_i}{d\tau} = \frac{\partial\mathcal{H}}{\partial p_i}, \quad \frac{dp_i}{d\tau} = -\frac{\partial\mathcal{H}}{\partial q_i}, \quad \frac{dT}{d\tau} = p_i\frac{\partial\mathcal{H}}{\partial p_i}, \qquad (2)$$

where both the Hamiltonian function $\mathcal{H}(\vec{q}, \vec{p}) = 1/2[\vec{p}^2 - u^2(\vec{q})\ (1 - \vec{p}.\vec{v}(\vec{q}))^2]$ and the sampling parameter τ are defined. An important conservation law could be deduced from the Eikonal: $\mathcal{H} = 0$ along an acoustic ray. We have introduced the sound slowness $u(\vec{q}) = 1/c(\vec{q})$. Each compo-

[1]Géosciences Azur, Université de Nice-Sophia Antipolis, Valbonne, France.
[2]Laboratoire de Physique, École Normale Supérieure, Lyon, France.
[3]Laboratoire de Détection et de Géophysique, Commisariàt à l'Energie Atomique, Bruyères le Châtel, France.
[4]Laboratoire Géosciences Marines, Institut de Physique du Globe de Paris, Paris, France.

0094-8276/04/2004GL020514

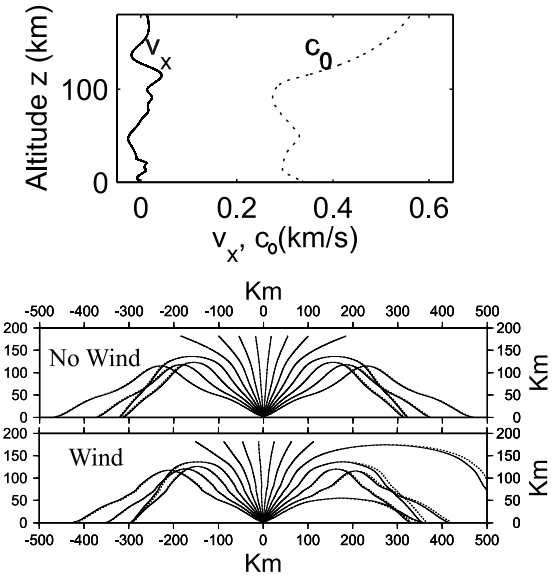

Figure 1. (top) Sound speed $c_0(z)$ and horizontal wind velocity $v_x(z)$ profiles from standard atmospheric models. Please note that the wind velocity may reach 20 m/s in the upper atmosphere. (bottom) Comparison between two numerical ray tracing: continuous line is for Garcès vertical integration and dashed line is for our scheme. Shooting angles vary from $-75°$ to $+75°$ with a step of $10°$.

nent of the wind is taken as positive when blowing towards positive direction. This ODE must be solved by numerical tools for a steady varying wind and for a variable sound velocity structure. Further approximations are possible leading to analytical investigations [*Abdullaev*, 1993].

3. Test Example With Realistic Sound and Wind Profiles

[8] Let us consider US Standard Atmosphere 1976 (USSA76) data for the sound celerity and wind data from an horizontal wind model [*Hedin et al.*, 1996] (Figure 1). Both sound velocity and horizontal wind variations are layered structures while the vertical wind component is negligible.

[9] Figure 1 shows the comparison of ray tracing (with and without horizontal wind) between *Garcès et al.* [1998] and our scheme. Differences in ray trajectories are quite small when no wind is present and are still negligible, although noticeable, when wind is present. These differences are coming essentially from different interpolation kernel of sound/wind velocity, especially when the ray is turning. Using the τ parameter instead of the z coordinate as sampling along the ray improves accuracy at turning points.

4. Laterally Varying Atmospheric Structure

[10] Because the wind velocity is a vectorial field, ray tracing depends on both wind amplitude and direction with respect to ray directions. We consider two illustrative situations.

4.1. Wind Velocity Influence

[11] Let us consider a simple unrealistic example for exhibiting the wind influence. For such illustration, a uniform sound celerity is considered where rays are straight lines in case of no winds. Let us assume a wind velocity with a fixed direction and an amplitude exponentially decaying from the center in (x, z) coordinates at $(-100$ km, 100 km) and (100 km, 100 km) with a maximal amplitude of 40 m/s. Arrows in Figure 2 show the direction of the wind. In spite of small amplitudes, the wind affects strongly ray trajectories when its direction is in the ray direction or in the opposite direction while little influence is observed for orthogonal ray directions. Focusing and defocusing by wind structures depend on the ray direction.

4.2. Wind Gradients Influence

[12] We now consider the standard sound velocity profile from the USSA76 profile (Figure 1). Ray tracing using this profile with no wind is presented in the top panel of Figure 3. We introduce an exponentially decaying local perturbation of the horizontal wind velocity which affects ray trajectories (middle panel of Figure 3) although the wind perturbation stays small (an average value below 10 m/s over a distance of 20 km with a peak value at the center of 40 m/s). We also perform ray tracing while considering similar perturbation on the vertical wind velocity component (the horizontal component is set to zero) as displayed in the bottom panel of Figure 3. In both cases, the sampling by rays of the atmosphere is different and illustrates that we need to take into account wind effects.

[13] This investigation of the influence of the wind velocity in atmospheric wave propagation shows that more precise models than the HWM93 [*Hedin et al.*, 1996] are required for better quantitative ray trajectory estimation and for accurate travel-times estimations.

5. Paraxial Ray Tracing Equations in a Moving Medium

[14] For computing the amplitude variation due to geometrical effects or equivalently the ray tube cross-section, we consider a slightly perturbed position $\vec{q}_0 + \delta\vec{q}$ with a slightly perturbed slowness vector $\vec{p}_0 + \delta\vec{p}$ as well as a

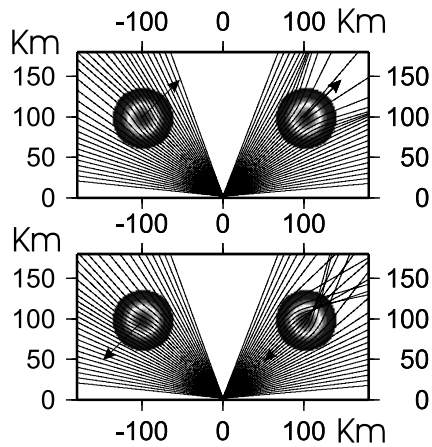

Figure 2. Illustrative interaction between straight rays and a small wind velocity field. Four cases are considered in this hypothetical medium. Arrows centered on the local wind anomaly show the direction of the wind which interacts quite differently depending where rays come from.

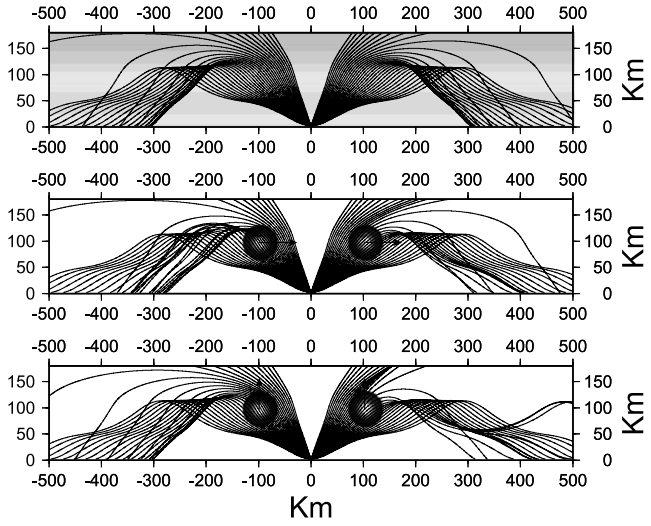

Figure 3. Influence of a local wind velocity variation over ray trajectories. The top panel presents ray trajectories for the USSA76 atmospheric model without wind. The gray background shows the velocity variation. The intermediate panel shows ray trajectories when an horizontal wind component is concentrated in two small areas (gray surfaces and arrows). The bottom panel presents ray trajectories when a vertical wind component is considered (gray surfaces and arrows). Please note the influence of the vertical wind in two rays going upward at the 50 km altitude.

slightly perturbed Hamiltonian function $\mathcal{H}_0 + (\partial_{\vec{q}}\mathcal{H})_0 \cdot \delta\vec{q} + (\partial_{\vec{p}}\mathcal{H})_0 \cdot \delta\vec{p}$ where the subscript 0 stands for a given ray along which we want to estimate the pressure amplitude. The deduced linearized equations for the perturbation vector $(\delta\vec{q}, \delta\vec{p})$ are

$$\begin{bmatrix} d\delta q_i/d\tau \\ d\delta p_i/d\tau \end{bmatrix} = \begin{bmatrix} \partial_p\partial_q\mathcal{H}_0 & \partial_p\partial_p\mathcal{H}_0 \\ -\partial_q\partial_q\mathcal{H}_0 & -\partial_q\partial_p\mathcal{H}_0 \end{bmatrix}_0 \begin{bmatrix} \delta q_i \\ \delta p_i \end{bmatrix} \qquad (3)$$

which could be solved by numerical means. Partial differentiations of the Hamiltonian function $\mathcal{H}$ are left to Appendix A.

[15] Initial conditions at the source depend on the problem at hand and we should consider them for both geometrical and paraxial rays. The estimation of ray tube requires the construction of the paraxial ray using only perturbation in the slowness vector and not in the source position itself. The quantity $(\partial_{\vec{p}}\mathcal{H})_0 \cdot \delta\vec{p}$ should be set to zero at the source to first-order and will stay constant while integration is performed along the ray. We define the point paraxial ray in a 2D geometry using this equation for initial values $\delta\vec{p}$ while $\delta\vec{q}$ are set to zero.

[16] Both systems (equation (2)) and (equation (3)) introduces new features compared to previously numerical ray tracing codes [*Garcès et al.*, 1998]. The Hamiltonian formulation allows one to build the paraxial equations and then gain access to geometrical amplitude variations while tracing rays by using Jacobian J for ray tube estimation [*Chapman*, 1985]. These equations are kept as simple as possible for fast numerical integration.

[17] We have found that the second-order Runge-Kutta scheme leads to fast and accurate integrations. Interpolations of both sound and wind velocity variations are performed by cardinal b-splines of order three in order to achieve an estimation of second derivatives for paraxial computations. The integration step τ is selected in order to achieve a relative variation of the Hamiltonian quantity of 10^{-3} s^2/m^2 along the longest ray.

6. Ray Amplitude Estimations Using the Paraxial Ray: Ground Impact Analysis

[18] The geometrical spreading may induce focusing and defocusing effects depending on the sound and wind spatial variations. Assuming that the flux of energy is preserved along a cross-section between rays as implied by the transport equation (thanks to Liouville theorem), i.e., that no energy leakage affects pressure estimation, the amplitude A is given by the expression $A(\tau_1) = F^{3/2}/2\pi r_0 1./\sqrt{\rho_1 u_1 |J_1|} e^{i\ \mathrm{KMAH}\pi/2}$ where the energy F is expressed as $\rho_0 u_0 J_0$ at the source and related to the amplitude A_0 estimated over a spherical shell of small radius r_0. The so-called KMAH is an integer equal to zero initially and which increases by one each time the ray hits a caustic [*Chapman*, 1985]. The density is denoted ρ_0 at the source and ρ_1 at the τ_1 position while the slowness is respectively given by u_0 and u_1.

[19] For the USSA76 sound velocity reference profile, we have estimated ray amplitude variation using both a finite difference procedure (a shooting angle increment θ equal to 10^{-2} and 10^{-3} make the aside independent ray, called numerical ray, near the main ray) and the paraxial formulation which does not need any angle increment. A unique ray with a shooting angle of 37° is drawn without no wind and with a uniform horizontal wind of 20 m/s (Figure 4). The numerical ray stays nearby the paraxial ray even when artificial amplification of ray tube is performed: the caustic zone when these rays cross the central ray is shifted by more than 100 km after 300 km of propagating distance. Focusing and defocusing are observed until the ray reaches a caustic where the amplitude becomes infinite: amplitude is only accurately determined by the paraxial formulation near the caustic while the finite difference technique depends critically on the angle increment.

[20] As opposed to the numerical strategy, the paraxial method is stable and faster in any case. Moreover, it allows continuous and local estimation of the amplitude along the ray and opens the road to the investigation of weak and strong non-linear effects when the sound velocity could depend on the amplitude of the wave vibration.

6.1. Amplitude Variations at Ground Impact Points

[21] Because recording stations are deployed on the ground, we have analyzed amplitude variations when ray is bouncing again and again at the Earth surface. For a punctual source, we have considered various winds. The Earth surface is hit at different points, showing the importance of an accurate estimation of the wind while the amplitude is controlled punctually by caustic zones. In spite of this very local effect, mean amplitude decay show consistent pattern although different for different winds. Amplitude ratio for models with wind with respect to the reference model without wind ranges between 0.7 and 1.2

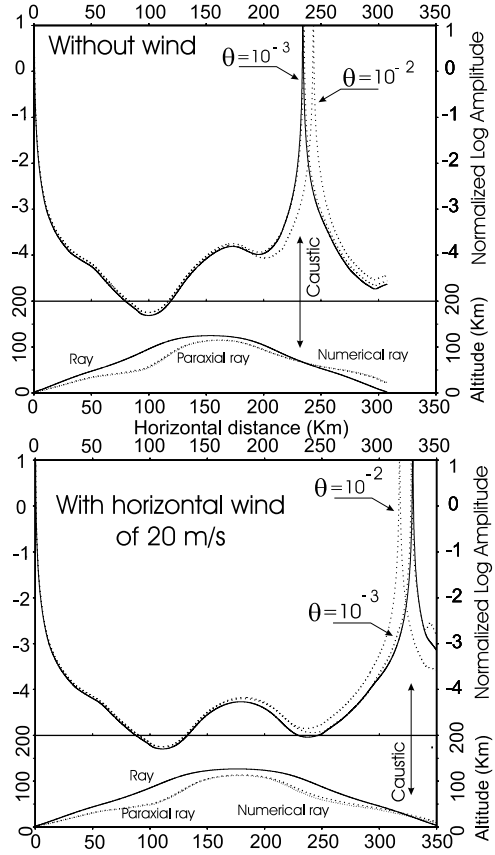

Figure 4. Amplitude variation and ray tracing without and with horizontal winds. On both panels, top box is the amplitude estimation while bottom box shows rays. Paraxial and numerical rays should overlap the central ray because angle increment is very small. Arbitrarily, the distance between these rays and the central ray has been amplified: caustic, detected when paraxial/numerical ray crosses the central ray, is shifted from 225 km to 325 km distance. Numerical amplitude estimations are quite accurate except near caustic zones where paraxial approach leads to superior results.

when ground stations are away from caustics. Therefore, one may hope to recover source features when these mean decays are correctly modelled by ray tracing on a significant number of ground stations in order to avoid caustic artefacts.

7. Conclusion

[22] The Hamiltonian formulation allows a systematic description of rays in the windy atmosphere. We have included non-homogeneous wind and sound velocities distributions in our formalism and we have constructed the two-dimensional numerical solution.

[23] We have estimated the geometrical variations of amplitude using the paraxial estimation rather than numerical differentiation between two neighbouring rays. Lateral variations of both the sound and the wind turn out to introduce noticeable modifications in the ray tracing itself as well as in the amplitude variation.

[24] We expect this amplitude estimation while tracing rays of great importance for non-linear estimation of sound velocity when it depends on the acoustic vibration itself. We have found as well that amplitude decay shows deterministic pattern making hope that statistical atmospheric models will be of interest for source estimation.

[25] Taking into account the impressive increase of infrasound measurements and the finer and finer description of the atmospheric properties, we believe that this interpretative tool will be useful for quantitative interpretation.

Appendix A: Partial Derivatives of the Hamiltonian

[26] Analytical expressions for the ray tracing and the paraxial ray tracing systems are

$$\frac{\partial H}{\partial q_i} = -\frac{1}{2}\Omega^2\frac{\partial u^2}{\partial q_i} + u^2\Omega p_l\frac{\partial v_l}{\partial q_i} \quad \frac{\partial H}{\partial p_i} = p_i + u^2\Omega v_i \tag{A1}$$

where we have written $\Omega = 1 - p_k v_k$ and used the Einstein notation, and

$$\begin{aligned}\frac{\partial^2 H}{\partial p_i \partial p_j} &= \delta_{ij} - v_i v_j u^2 \quad \frac{\partial^2 H}{\partial p_i \partial q_j} = u^2\Omega\frac{\partial v_i}{\partial q_j} + \Omega v_i\frac{\partial u^2}{\partial q_j} - u^2 v_i p_k\frac{\partial v_k}{\partial q_j}\\ \frac{\partial^2 H}{\partial q_i \partial q_j} &= -\frac{1}{2}\Omega^2\frac{\partial^2 u^2}{\partial q_i \partial q_j} + \Omega\frac{\partial u^2}{\partial q_i}p_l\frac{\partial v_l}{\partial q_j} + \Omega\frac{\partial u^2}{\partial q_j}p_l\frac{\partial v_l}{\partial q_i}\\ &\quad - u^2\left(p_l\frac{\partial v_l}{\partial q_j}\right)\left(p_l\frac{\partial v_l}{\partial q_i}\right) + u^2\Omega p_l\frac{\partial^2 v_l}{\partial q_i \partial q_j}\end{aligned} \tag{A2}$$

[27] The Hamiltonian formulation allows a systematic construction of the system of partial differential equations.

[28] **Acknowledgments.** Many thanks to Alexis Le Pichon for the Garcès ray tracing software called HAWAI and to Maud Barthélémy for a preliminary work. Careful reviews by Juliette Artru and Bernard Minster have improved the manuscript. Partial financial support has been provided by DASE/CEA through contract n^0 460009 3805/P6H53. Contribution Géosciences Azur n^0 536.

References

Abdullaev, S. (1993), *Chaos and Dynamics of Rays in Waveguide Media*, Gordon and Breach, Newark, N. J.

Artru, J., P. Lognonné, and E. Blanc (2001), Normal modes modelling of post-seismic ionospheric oscillations, *Geophys. Res. Lett.*, *28*, 697–700.

Calais, E., and J. Minster (1996), GPS detection of ionospheric perturbations following a space shuttle ascent, *Geophys. Res. Lett.*, *23*, 1897–1900.

Chapman, C. (1985), Ray theory and its extension: WKBJ and Maslov seismograms, *J. Geophys.*, *58*, 27–43.

Christie, D. (1999), The infrasonic segment of the CTBTO's international monitoring system, paper presented at International Union of Geodesy and Geophysics XXII General Assembly, Birmingham, U. K.

Courant, R., and F. John (1966), *Introduction to Calculus and Analysis*, Wiley-Interscience, New York.

Farges, T., A. Le Pichon, E. Blanc, S. Perez, and B. Alcoverro (2003), Response of the lower atmosphere and the ionosphere to the eclipse of August 11, 1999, *J. Atmos. Sol. Terr. Phys.*, *65*, 717–726.

Garcès, M., R. Hansen, and K. Lindquist (1998), Traveltimes for infrasonic waves propagating in a stratified atmosphere, *Geophys. J. Int.*, *135*, 255–263.

Hedin, A., et al. (1996), Empirical wind model for the upper, middle and lower atmosphere, *J. Atmos. Terr. Phys.*, *58*, 1421–1447.

Le Pichon, A., M. Garcès, E. Blanc, M. Barthelemy, and D. Drob (2002a), Acoustic propagation and atmosphere characteristics derived from infrasonic waves generated by the Concorde, *J. Acoust. Soc. Am.*, *111*, 629–640.

Le Pichon, A., J. M. Guérin, E. Blanc, and D. Reymond (2002b), Trail in the atmosphere of the 29 December 2000 meteor as recorded in Tahiti:

Characteristics and trajectory reconstitution, *J. Geophys. Res.*, *107*(D23), 4709, doi:10.1029/2001JD001283.

E. Blanc, Laboratoire de Détection et de Géophysique, Commisariàt à l'Energie Atomique, Bruyères le Châtel, France.

J.-X. Dessa, Laboratoire Géosciences Marines, Institut de Physique du Globe de Paris, Paris, France.

N. Garnier, Laboratoire de Physique, École Normale Supérieure, Lyon, France.

J. Virieux, UMR-Geosciences Azur, Université de Nice-Sophia Antipolis, 250 Rue Albert Einstein, F-06560 Valbonne, France. (viri@geoazur.unice.fr)